

# PCCP

Accepted Manuscript



This is an *Accepted Manuscript*, which has been through the Royal Society of Chemistry peer review process and has been accepted for publication.

*Accepted Manuscripts* are published online shortly after acceptance, before technical editing, formatting and proof reading. Using this free service, authors can make their results available to the community, in citable form, before we publish the edited article. We will replace this *Accepted Manuscript* with the edited and formatted *Advance Article* as soon as it is available.

You can find more information about *Accepted Manuscripts* in the [Information for Authors](#).

Please note that technical editing may introduce minor changes to the text and/or graphics, which may alter content. The journal's standard [Terms & Conditions](#) and the [Ethical guidelines](#) still apply. In no event shall the Royal Society of Chemistry be held responsible for any errors or omissions in this *Accepted Manuscript* or any consequences arising from the use of any information it contains.

# Identification of Emitting Molecular Species by Time-Resolved Fluorescence Applied to Excited State Dynamics of Pigment Yellow 101

Seung Noh Lee,<sup>a</sup> Jaeheung Park,<sup>b</sup> Manho Lim<sup>\*b</sup> and Taiha Joo<sup>\*a</sup>

Received 00th January 2012,

Accepted 00th January 2012

DOI: 10.1039/x0xx00000x

www.rsc.org/

Time-resolved fluorescence (TRF) with a resolution higher than the periods of vibrations may provide the vibrational spectrum of an emitting species by directly recording the vibrational wave packet motions in time. We applied high-resolution TRF to investigate the excited-state dynamics of pigment yellow 101 (P.Y.101). The TRF spectra of P.Y.101 in dichloromethane showed that upon photoexcitation of the enol isomer, dynamics occur in  $S_1$  state to form a product in two time constants at 30 and 140 fs. TRF signals were modulated due to the vibrational wave packet motions in the excited states, which provided the vibrational spectra of the emitting species. Depending on the emission wavelength, two different vibrational spectra were evident. With the help of theoretical calculations, the two spectra were assigned to the enol and keto isomers of P.Y.101 in the  $S_1$  state, leading to the conclusion that P.Y.101 undergoes ultrafast excited-state intramolecular proton transfer (ESIPT) with a quantum yield close to 1. Visible-pump infrared-probe transient absorption spectra were recorded to corroborate this conclusion.

## 1. Introduction

Electronic transitions of polyatomic molecules in liquid are generally characterized by a broad featureless band that represents superposition of vibronic transitions consisting of progressions in Franck-Condon active vibrations. Each vibronic transition undergoes line-broadening processes of time scales ranging from femtoseconds to nanoseconds.<sup>1</sup> The line broadening processes and vibronic structures can be decoded via time-resolved spectroscopies such as transient absorption (TA),<sup>2,3</sup> 3 pulse photon echo peak shifts (3PEPS),<sup>1,4</sup> and time-resolved fluorescence (TRF),<sup>5</sup> to provide the structure and dynamics of a molecule in a specific electronic state. TRF has a unique advantage over TA and other nonlinear spectroscopies that are based on molecular resonances, as a TRF signal comes from the excited state exclusively. By tuning the probe wavelengths longer than the first ground state absorption, TA may also probe the excited state exclusively through the excited state absorption.<sup>6</sup> The time resolution of a TRF apparatus, however, is usually not high enough to provide molecular information of the emitting species through the vibronic structures that can be attained by resolving the coherent nuclear wave packet motions.

Excited state intramolecular proton transfer (ESIPT) has been employed as one of the model systems for studies of the proton transfer dynamics.<sup>7-10</sup> In an ESIPT reaction, a proton migrates from the donor (usually a hydroxyl group) to an

acceptor (usually a nitrogen or oxygen atom) in an electronic excited state to form a keto isomer with an intramolecular hydrogen bond. In general, ESIPT is ultrafast occurring in less than 100 fs to result in absence of emission from the reactant, the enol isomer, which in turn results in a large Stokes shift ranging from 6000 to 10000  $\text{cm}^{-1}$ .<sup>7</sup> Some ESIPT molecules may form intermolecular hydrogen bonding with solvents or impurities such as water, which may then produce a strong enol emission.<sup>11,12</sup>

2,2'-Dihydroxy-1,1'-naphthalazine, known as pigment yellow 101 (P.Y.101), is a fluorescent dye used for mass coloration of viscose.<sup>13,14</sup> It forms two six-membered ring structures via intramolecular hydrogen bonding as shown in scheme 1, which may enable ESIPT. The dynamics of P.Y.101 in the excited ( $S_1$ ) state have been reported previously.<sup>15-17</sup> Lorenz et al. reported in a visible pump/probe TA study that upon photoexcitation of P.Y.101 in dichloromethane, a major part of the excited state population undergoes radiative relaxation to the ground state, and to a minor extent undergoes ESIPT to become a keto isomer.<sup>15</sup> A minor part of the keto isomer undergoes further conformational dynamics to the cis-isomer in the  $S_1$  state.



Scheme 1 ESIPT scheme of P.Y.101 from trans-diol to trans-keto.

For P.Y.101 in solid state, quantum mechanical calculations showed that  $\pi$ - $\pi^*$  is the lowest energy transition with high oscillator strength,<sup>12,13,16</sup> and a TA study showed that part of the enol isomer undergoes ESIPT without trans-cis isomerization.<sup>16</sup>

In this work, we measured TRF of P.Y.101 in dichloromethane to investigate the dynamics in the excited state. ESIPT typically occurs much faster than 100 fs, which can result in an impulsive excitation of the product vibrational modes.<sup>18-24</sup> By employing TRF at a high enough time resolution, we attempted to identify the emitting chemical species through the wave packet motions in the excited states as well as to reveal their dynamics. A visible-pump infrared-probe TA (IRTA) study was also presented to corroborate our conclusion.

## 2. Materials and methods

The light source for the TRF measurements was a home-made cavity-dumped Ti:sapphire laser operating at a repetition rate of 350 kHz. The laser spectrum was tuned to generate 25 fs pulses at 800 nm. Pump pulses at 400 nm were generated by the second harmonic generation in a 50  $\mu$ m thick BBO crystal. Details of the femtosecond TRF apparatus utilizing non-collinear sum frequency generation (SFG) and a Cassegrain reflector were reported previously.<sup>25</sup> The TRF spectra (TRFS) were measured without resorting to the conventional spectral reconstruction method. The detection monochromator, phase matching angle of the BBO crystal for the SFG, and the gate delay, which compensates the group velocity dispersion due to the sample cuvette and collection optics, were scanned synchronously.<sup>5</sup> Time resolutions (full width at half maximum, FWHM) for the TRF and TRFS were estimated by the SFG between the gate pulse and the Raman scattering from the solvent to be 50 and 80 fs, respectively. Picosecond TRF was measured by the time correlated single photon counting (TCSPC) method. Details of the TCSPC apparatus providing 60 ps (FWHM) time resolution by employing a single photon silicon avalanche photodiode (id100-50, ID Quantique) were reported previously.<sup>26</sup>

Details of the visible-pump infrared-probe TA apparatus with a 64-element HgCdTe detector were described elsewhere.<sup>27</sup> The light source was an amplified Ti:sapphire laser system (Hurricane, Spectra Physics) generating 110 fs pulses at 800 nm at 1 kHz. A home-made optical parametric amplifier was used to generate mid-infrared pulses. Infrared detection was performed across the 1400 to 1700  $\text{cm}^{-1}$  region, which corresponds to the N-H bending and C=O stretching frequencies of the keto isomer. The time resolution was 180 fs.

Stationary absorption and emission spectra were measured by a UV-Visible spectrophotometer (S-3100, Scinco) and a fluorometer (Photon Technology International), respectively. A CCD (RTE/CCD-128-HB, Roper Scientific) detector with laser excitation was also employed for the fluorescence spectra measurement.

P.Y.101, dichloromethane, and toluene were purchased from Sigma-Aldrich at the highest purities, and used without further purification. For the TRF measurements, a 3 mM solution of P.Y.101 in dichloromethane was prepared in a 100  $\mu$ m

pathlength fused silica flow cell. Photodamage of the sample was minimized by shaking the flow cell. For the IRTA experiment, the sample solution was loaded in a home-made spinning cell. The sample cell was rotated sufficiently fast so that each laser pulse excited a fresh volume of the sample. All measurements were carried out at ambient temperature ( $24 \pm 1$  °C).

Theoretical calculations were performed using the Gaussian 09 quantum chemistry calculation package.<sup>28</sup> Density functional theory (DFT) and time-dependent DFT (TDDFT) with a 6-31G basis set were used for the calculations of the ground and excited states, respectively. Since significant charge transfer is involved for the ESIPT process of P.Y.101, the B3LYP hybrid functional which has a 50 % Hartree-Fock exchange was used to remedy the charge-transfer problem in TDDFT.<sup>17,29</sup> Vibrational frequencies from the DFT calculation were scaled by literature values; 0.948 for below 500  $\text{cm}^{-1}$  and 0.924 for above 1000  $\text{cm}^{-1}$ .<sup>30</sup> Excited state vibrational frequencies from TDDFT in the 1400–1700  $\text{cm}^{-1}$  region were scaled by 0.912, chosen arbitrarily to match the infrared absorption bands. Displacements and the reorganization energies for the vibrational modes between two relevant electronic states were calculated as described in the literature.<sup>31</sup>

## 3. Results and discussion

### 3.1 Stationary Spectra

The absorption and fluorescence spectra of P.Y.101 in dichloromethane do not exhibit the mirror image, which implies that the structures of the ground and excited states are different (Fig. 1). The Stokes shift calculated from the absorption and fluorescence maxima at 411 and 512 nm, respectively, is 4800  $\text{cm}^{-1}$ . The Stokes shift is much smaller than that of typical ESIPT molecules such as 2-(2'-hydroxyphenyl)benzothiazole (HBT) and 10-hydroxybenzo[h]quinoline (HBQ), where the fluorescence from the enol isomers are absent because of the ultrafast ESIPT.<sup>22</sup> In fact, the 512 nm band was assigned to fluorescence from the enol isomer.<sup>13,15</sup> In that case, the shoulder at 550 nm in the fluorescence spectrum is most likely due to a vibrational progression. If this is true, then the ESIPT of P.Y.101 must be much slower than the population relaxation of the enol isomer due to the unfavourable energetics or conformation for ESIPT including the possibility of intermolecular hydrogen

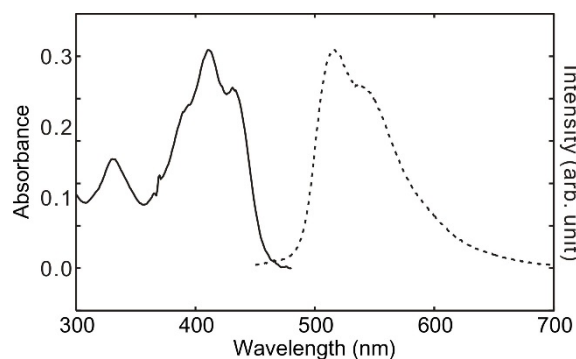


Fig. 1 Absorption (solid line, left axis) and fluorescence (dashed line, right axis) spectra of P.Y.101 in dichloromethane.

bonding with the solvent.<sup>11</sup> The fluorescence spectra of P.Y.101 in dichloromethane, toluene, and their water-saturated solutions (data not shown) were identical, indicating that the effect of solvent polarity is negligible and that the possibility of intermolecular hydrogen bonding with solvent is insignificant.

### 3.2 Time-Resolved Fluorescence

**3.2.1 TRF SPECTRA.** Stationary fluorescence from the enol isomers of HBQ and HBT is absent, because the ESIPT rates are ultrafast, much faster than 100 fs.<sup>20-22,32,33</sup> However, TRF is capable of capturing the fluorescence from the enol isomers of HBQ and HBT.<sup>22</sup> Analogously, provided that P.Y.101 undergoes ultrafast ESIPT, the 512 nm band should arise from the keto isomer, and the enol fluorescence is expected to appear at approximately 470 nm. The dynamics in the excited state in general can be best examined by TRFS because a TRF signal at a fixed wavelength is affected by spectral relaxation processes such as solvation and vibronic relaxation as well as population relaxation.

Fig. 2 shows the TRFS measured at several time delays. Instrument limited rise was observed for the first 50 fs over a broad spectral range from 440 to 580 nm, although the rise at the high frequency side is slightly faster. The intensity of the high frequency side then decayed quickly over the first ~300 fs, and then somewhat slowly at later times. After approximately 1 ps, the TRFS is similar to the stationary fluorescence spectrum of P.Y.101, and the intensity decays in tens of picosecond time scale while the shape is mostly uniform.

Time-resolved area-normalized emission spectra (TRANES) can often be a useful way to illustrate the overall dynamics.<sup>34,35</sup> It has been well established by mathematical analysis that TRANES can be used to examine the number of emissive states in TRFS. Analogous to the isosbestic point in absorption spectra, an isoemissive point in TRANES indicates the presence of two emissive species. The TRANES obtained in the current work displayed an isoemissive point at 503 nm, indicating that two emitting species existed following the photoexcitation (Fig. 2b).

To assign the two emitting species (states) observed in the TRFS, molecular conformations in the ground state first needed to be considered. Plötner and Dreuw applied DFT calculations and reported that several different molecular conformations are possible in the ground state, including trans-diol (Scheme 1), trans-keto (Scheme 1), trans-diketeto, cis-diol, and cis-keto.<sup>16</sup> Among these isomers, trans-diol is the lowest in energy by 2000  $\text{cm}^{-1}$  compared to the next lowest-energy isomer, which could be cis-diol or trans-keto. Therefore, trans-diol should be the only significantly populated isomer in the ground state, and the chemical species created immediately by the photoexcitation, which emits in the 440–510 nm region, should be trans-diol in the  $S_1$  state. Because the TRANES observed in the current study clearly showed that the initial photoexcited state quickly converts to a different species (state), we should assign the fluorescence band at 500–570 nm to an isomer other than trans-diol, even though trans-diol was reported to be the lowest-energy isomer in  $S_1$  manifold.<sup>17</sup> We propose that the fluorescence band at 500–570 nm arises from the trans-keto isomer. In fact, in our

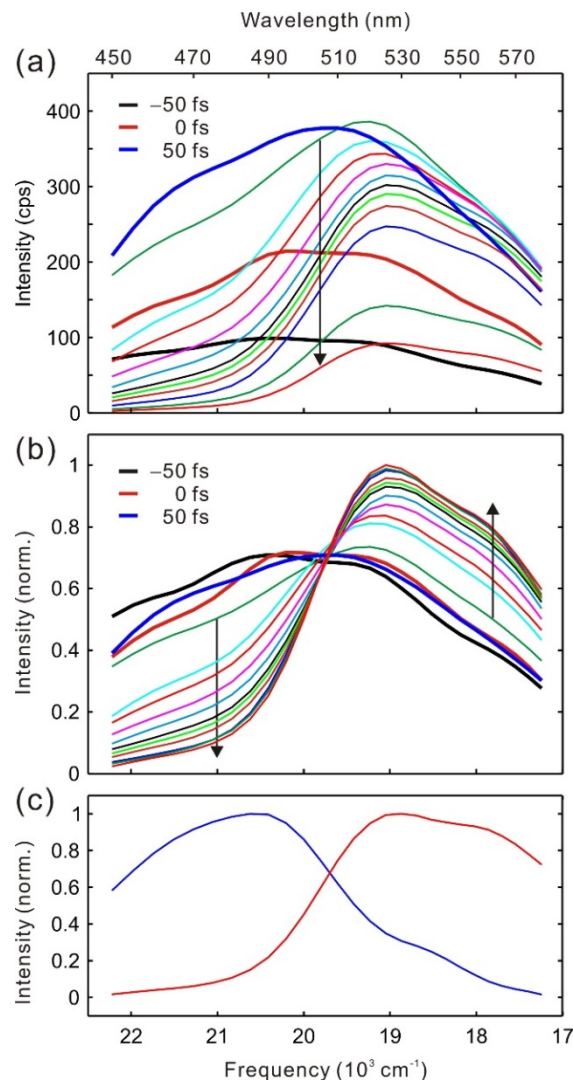


**Fig. 2** (a) TRFS and (b) area normalized TRFS. The three thick lines are TRFS at -50 fs (black), 0 fs (red), and 50 fs (blue). Following the directions of arrows, times are 100 fs, 200 fs, 300 fs, 500 fs, 1 ps, 2 ps, 3 ps, 5 ps, 10 ps, 40 ps and 80 ps. TRFS were 3 points smoothed for easy reading. (c) Fluorescence spectra of the enol and keto isomers obtained by decomposition of the TRFS.

TDDFT calculation, where the molecule was restricted to be planar, the energy of the trans-keto isomer lies 150  $\text{cm}^{-1}$  below that of trans-diol in  $S_1$ . Isomers other than trans-diol and trans-keto were reported to be significantly higher in energy by at least 2000  $\text{cm}^{-1}$  in the excited state.<sup>17</sup> It should be noted that double proton transfer cannot take place, since trans-diketeto is ~2000  $\text{cm}^{-1}$  higher than trans-keto in  $S_1$ .<sup>17</sup> Note also that it should take much longer than the population relaxation time (~1 ps) of the trans-diol for the N–N bond to rotate by 180° to become a cis isomer. Hereafter, the trans-diol and trans-keto isomers are simply called the enol and keto isomers, respectively.

TRFS can be decomposed into two parts, the enol and keto fluorescence spectra. The TRFS at extended time (80 ps) was assigned to the fluorescence spectrum of the keto isomer, and the enol spectrum was obtained by subtracting the keto spectrum from the TRFS at 100–300 fs (Fig. 2c). Amplitudes of each part of the spectrum were obtained from TRFS and fitted to a sum of

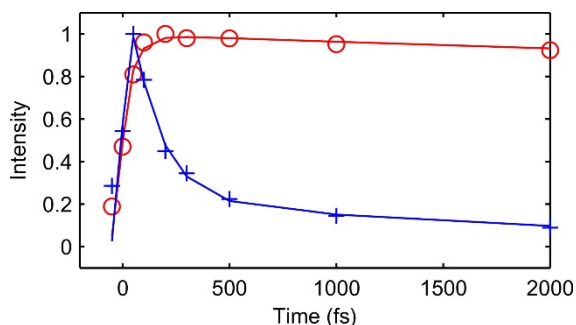


Fig. 3 Amplitudes of the enol (blue) and keto (red) fluorescence from TRFS.

exponentials (Fig. 3). Fluorescence of the enol isomer decays by two time constants at 140 fs (84 %) and 2.3 ps (16 %), whereas the keto fluorescence rises by 50 fs and decays biexponentially by 3.3 ps (14 %) and 64 ps (86 %). The femtosecond components may reflect the ESIPT rates. Due to the limited number of data points and the lower time resolution for the TRFS measurement, however, the femtosecond time constants were not well determined in the TRFS, and we will not use these numbers for the discussion of the ESIPT dynamics. Detailed discussion on the ESIPT dynamics will be made in the next section using the TRF results.

The 64 ps time constant can be assigned to the population relaxation time of the excited keto isomer to the ground state, as it represents the ground state recovery (see section 3.3). Origins of the other two picosecond components are not certain. The 2.3 ps decay of the enol isomer may reflect the ESIPT dynamics or the internal conversion of the enol isomer to the ground state. A corresponding rise of the keto fluorescence was not observed, which contradicts the former, and picosecond ground state recovery also was not observed (see section 3.3), which contradicts the latter. Regardless, a small part of the excited enol isomer survives for a few picoseconds, which allows for observation of the vibrational wave packet motion of the excited enol isomer. Lorenz et al. reported a TA study of P.Y.101 in dichloromethane in the visible region with a time resolution of 150 fs.<sup>15</sup> From the global analysis, they extracted five time constants of 150 fs, 4.7 ps, 63 ps, 500 ps, and infinity. Among these, 150 fs and 63 ps were the two dominant components, which agrees with the present experiment. They interpreted that the 150 fs time constant reflects the initial spreading of the Franck-Condon wave packet to populate mostly the enol isomer and to a minor extent the keto isomer, and the 63 ps time constant reflects the radiative decay of the enol isomer.<sup>15</sup>

**3.2.2 TRF AT SELECTED WAVELENGTHS.** To scrutinize the ESIPT rates and the wave packet dynamics, TRF was measured at selected wavelengths. We first obtained the survey TRF in picosecond time resolution by TCSPC (Fig. S1, ESI). Picosecond TRF signals are nearly the same at all wavelengths from 470 to 550 nm, and decayed mostly by a single exponential of time constant 67 ps.<sup>36</sup> A small amplitude (2 %) 860 ps component is also present, and its amplitude increases at longer wavelengths.

The femtosecond TRF was measured at selected wavelengths (Fig. 4), and the results were nonlinear least square fitted to a

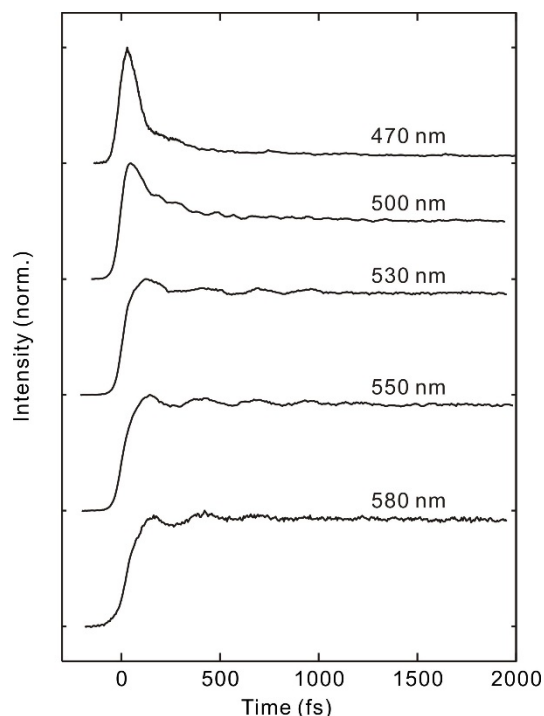


Fig. 4 TRF of P.Y.101 in dichloromethane measured at selected wavelengths.

sum of exponentials (Table 1). At 470 nm, where the fluorescence from the enol isomer is expected to be dominant, the TRF decays mostly by 33 and 160 fs. A small 1.2 ps component is present along with the 67 ps component, which is attributed to the keto fluorescence extending to 470 nm as evident from the picosecond TRF. At longer wavelengths, TRF rise by  $\sim 30$  fs. At 500 nm, the rise seems to be faster and this was possibly due to the interference from the wave packets. At 550 nm, it rises by two time constants at 30 and 150 fs, which are similar to the TRF decay at 470 nm. At 580 nm the rise is slower and appeared to be a single exponential with a time constant of 86 fs, which is similar to the average of the two rise time constants at 550 nm. The slower rise at 580 nm may have been caused by the vibronic relaxation, although the TRFS indicate that the effect may not be significant. Because the ESIPT reaction is accompanied by a dipole moment change of 1.02 D,<sup>17</sup> the TRF at 580 nm, which is at the red edge of the keto fluorescence spectrum, may have also been affected by solvation dynamics. The dipolar solvation times of dichloromethane determined by the Stokes shift of coumarin 153 are 144 fs and 1.02 ps.<sup>37</sup> Note that the  $\tau_2$  component in TRF should be interpreted as the excited-state population dynamics, not as the

**Table 1** Results of the nonlinear least square fits to a sum of exponentials for the TRF signals at fixed wavelengths. Negative amplitudes indicate rise.

$\lambda$ (nm)	$A_1$	$\tau_1$ (fs)	$A_2$	$\tau_2$ (fs)	$A_3$	$\tau_3$ (ps)	$A_4$	$\tau_4$ (ps) <sup>1)</sup>
470	0.54	35	0.39	140	0.04	1.2	0.03	67
500	-1	20	0.58	130	0.06	2.0	0.36	67
530	-1	34	0.24	120			0.76	67
550	-0.83	30	-0.17	150	0.03	13	0.97	67
580	-1	86					1	67

<sup>1)</sup> Fixed to a value obtained from an extended time scan.

solvation dynamics, because the 140 fs component also occurred in the TRFS as an intensity change, not a frequency shift. It should also be noted that TRFS measurements of the enol fluorescence contains the 2.3 ps decay. By taking into account the TRF and TRFS results, we concluded that the ESIPT rate of P.Y.101 in dichloromethane can be characterized by two time constants at  $30 \pm 10$  and  $140 \pm 20$  fs. It is not clear if the origin of the  $\tau_3$  component, which also appeared in the TRFS, is part of the ESIPT or other dynamics occurring in the enol and keto isomers in the excited state, including conformational dynamics and internal conversion from  $S_1$  to the ground state.

**3.2.3 WAVE PACKET DYNAMICS.** Modulations of the TRF signals were observed and appeared to vary at different wavelengths (Fig. 4). An impulsive excitation, for example, a Franck-Condon transition by a short pulse of light creates coherent nuclear wave packets whose amplitudes are proportional to the electron-nuclear coupling (Huang-Rhys factor). It has also been well established that an ultrafast chemical reaction can act as an impulsive excitation of the vibrations of the product.<sup>18-24</sup> These vibrational wave packet motions appear as modulations in TA and in TRF signals. Because fluorescence from an excited state is detected in TRF, it follows that a TRF signal comes from the chemical species in the excited state. In a TRF experiment, the detection wavelength can also be tuned to either the reactant or product fluorescence to selectively detect each chemical species. In a TA experiment, however, an oscillation may originate in general from the wave packet motions in the ground and excited states of the reactant and products, and therefore it cannot be assigned to a specific

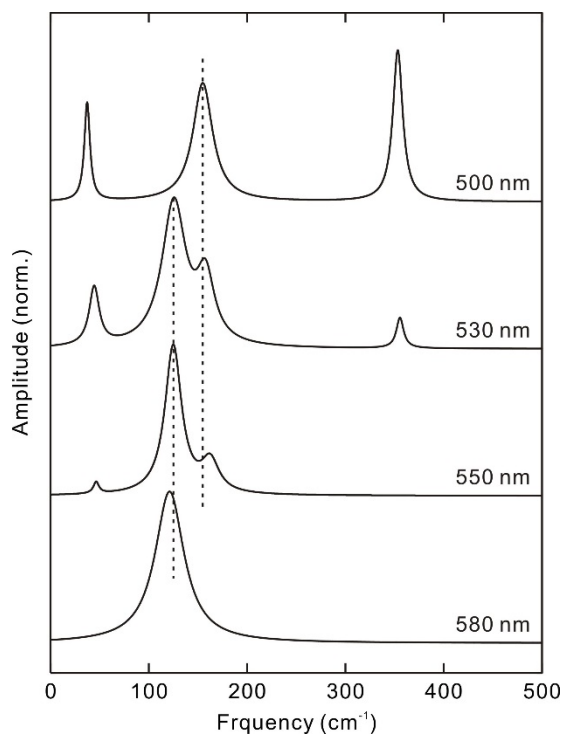


**Fig. 5** The oscillation spectra in TRFs at different detection wavelengths obtained by LPSVD method.

**Table 2.** Oscillation frequencies ( $\text{cm}^{-1}$ ) from TRF obtained by LPSVD method and their assignments to the normal modes of P.Y.101 enol and keto isomers in the excited states.

Mode*	500 nm	530 nm	550 nm	580 nm	Calc.*
$\nu_3$	37	45	47		35 (35)
$\nu_7$		125	123	122	123 (124)
$\nu_{10}$	155	158	163		160 (155)
$\nu_{17}(\nu_{18})$	354	355			350 (356)

\* Numbers in parentheses are associated with the excited keto isomer.

state or chemical species,<sup>38,39</sup> unless the TA signal is shown to originate from only one transition.

The oscillation frequencies were obtained by employing both the Fourier transform of the residual of the exponential fits (Fig. S2, ESI) and linear prediction singular value decomposition (LPSVD) methods.<sup>40-42</sup> Although the two methods produced essentially the same results, we used the LPSVD method since it gives correct amplitudes of the oscillations. Because of the varying phase for each vibrational mode, application of the Fourier power spectrum is required where the amplitudes are not scaled properly. The oscillation spectra from the TRF at different wavelengths are shown in Fig. 5, and the frequencies are listed in Table 2. At 500 nm, three peaks are evident at 37, 155, and  $354 \text{ cm}^{-1}$ , and the spectrum changes gradually to a single peak at  $123 \text{ cm}^{-1}$  as the detection wavelength increases. Combined with the TRFS and the theoretical calculations described below, we assigned the spectrum at the short wavelength (500 nm) to the vibrations of the enol isomer in the  $S_1$  state and the spectrum at the long wavelength (580 nm) to the vibrations of the keto isomer in the  $S_1$  state. For the intermediate wavelengths, the spectrum is a sum of the two contributions. The oscillation spectrum for the TRF at 470 nm could not be obtained reliably partly due to the rapid decrease of the TRF intensity by ESIPT. However, significant oscillation amplitudes are expected, based on the observed enol fluorescence spectrum (Fig 2c). The reason for the very weak modulation at 470 nm is attributed to the detection wavelength being near the centre of the enol fluorescence spectrum. A TRF (and TA) signal intensity is least sensitive to the wave packet motion when detected at the centre of the fluorescence peak, because modulation of the TRF signal arises from the oscillation of the centre frequency of the fluorescence spectrum as a function of time by the wave packet motion.

The coherent vibrational wave packets created in the product potential energy surface (PES) can provide critical information on the reaction mechanism and molecular dynamics as demonstrated for the ESIPT of HBQ and HBT.<sup>19-22</sup> The coherent vibrational wave packets on the product PES can be best calculated once the full excited-state PES is known. Schriever et al. constructed the  $S_1$  PES and performed classical dynamics simulations to extract the vibrational modes that would be coherently excited as a result of the ultrafast ESIPT reactions for HBQ and HBT.<sup>32</sup> Higashi and Saito used the multi-configuration Shepard interpolation method to construct the PES and performed molecular dynamics simulations to calculate the vibrational excitations in the product keto isomer of HBQ.<sup>43</sup> De Vivie-Riedle et al. presented a more efficient method for the

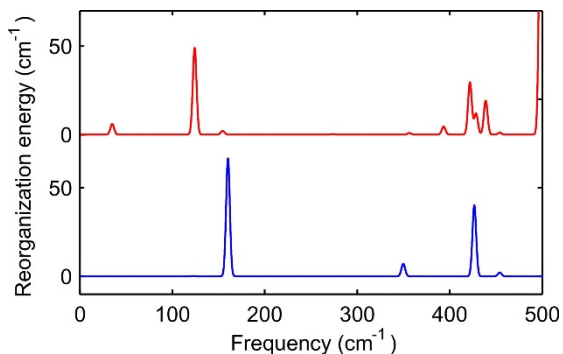


**Fig. 6** Calculated reorganization energies for the  $S_0 \rightarrow S_1$  transition of the enol isomer (blue), and transition from enol  $S_1$  to keto  $S_1$  (red).

determination of the active modes in vibronic wave packets through the normal-mode analysis along the reaction path.<sup>44</sup> Kim and Joo calculated the reaction Huang-Rhys factors (RHRF) by the projection of the displacements between the reactant and product onto the normal modes of the product by assuming instantaneous chemical reaction.<sup>22</sup> Excellent agreement between theories and experiments has been reported for the ESIPT of HBT and HBQ, although the role of hydrogen remains controversial.<sup>32,43,45</sup>

We have calculated RHRF to obtain the oscillation spectra of the enol and keto isomers from TRF. The oscillation spectrum for the enol isomer can be calculated from the displacement between the enol ground and enol excited states. For the keto isomer, the displacement between the ground enol and excited keto isomers was calculated to produce the spectrum. Molecular structures and vibrational spectra were calculated by DFT and TDDFT methods using the B3LYP functional. Local minima for both enol and keto excited states were observed, which indicates a finite barrier for the ESIPT, with the keto isomer present 150  $\text{cm}^{-1}$  below the enol isomer. Displacements between the two relevant structures were calculated and projected onto the normal modes of the final states to obtain the RHRF. Within the Condon approximation, the modulation amplitude is determined by the magnitude of the fluorescence centre frequency swing, which in turn is proportional to the vibrational reorganization energy. To compare the theoretical calculations to the experimental results, the corresponding vibrational reorganization energies ( $\lambda_{\text{vib}} = \hbar\omega\delta^2/2$ ) were calculated (Fig. 6), where  $\delta$  is the projection amplitude,  $S = \delta^2/2$  is the Huang-Rhys factor, and  $\omega$  is the vibrational frequency (also listed in Table 2).

The absence of high frequency ( $>400 \text{ cm}^{-1}$ ) vibrations are apparent on the TRF oscillation spectra (Fig. 5). The upper frequency limit that can be observed in the experiment may be determined by two factors: the time resolution of the experiment and the ESIPT rate. Because of the finite time resolution, an oscillation of frequency  $\omega$  is attenuated by a factor  $\exp(-\sigma^2\omega^2/2)$ , where  $\sigma$  is the standard deviation of the instrument response function assuming Gaussian. For the present experiment, the 300  $\text{cm}^{-1}$  vibrational mode was attenuated by a factor of 2, and the 415  $\text{cm}^{-1}$  mode by a factor of 4. The TRF of the enol isomer was limited only by the experimental time resolution, since the Franck-Condon transition is essentially instantaneous. For the

keto isomer, however, it is not straightforward to determine the limiting factor, since it is reaction mechanism dependent. For the purely statistical (Markovian) dynamics, wave packets for the vibrational mode having periods shorter than the ESIPT time cannot be created. However, for a reaction that can be described by the ballistic motion along the reaction coordinate such as the ESIPT, wave packet motions with periods shorter than ESIPT time could still be observed. Since the major component of the ESIPT dynamics (30 fs) is faster than the instrument response, we expect that the effect of the finite ESIPT rate is minor, if any, for the upper frequency limit.

All of the frequencies observed in the experiment displayed nonzero reorganization energies from the calculations. More importantly, these are the only vibrational modes having nonzero reorganization energies below 400  $\text{cm}^{-1}$ , which demonstrates the validity of the theory. The 155 and 354  $\text{cm}^{-1}$  modes are present in both experiment and calculation for the enol isomer which demonstrated excellent agreement between the theory and experiment, although the amplitude of the 354  $\text{cm}^{-1}$  mode in the calculation is smaller than that observed in the experiment. The 37  $\text{cm}^{-1}$  mode is prominent at short wavelengths implying that it arises from the enol isomer, yet it is absent in the calculation. The 123  $\text{cm}^{-1}$  mode is prominent in the long wavelength spectra and is present only in the keto isomer, again demonstrating excellent agreement between theory and experiment. The overall agreement between the experiment and calculation is excellent. Furthermore, it demonstrates that TRF with high enough time resolution used in combination with theoretical calculations can be utilized for the identification of the emitting chemical species through the wave packet motions in the excited state, an attribute that is normally unavailable in fluorescence spectroscopy. A similar concept has been demonstrated with femtosecond stimulated Raman spectroscopy (FSRS),<sup>46</sup> and recently applied to the excited-state intermolecular proton transfer of pyranine.<sup>47</sup>

All four modes listed in Table 2 are in-plane vibrations. For the barrierless ESIPT by the skeletal deformation model, in-plane skeletal vibrations that shorten the O–N distance will be excited preferentially in the product PES.<sup>33</sup> The  $\nu_7$  mode, which is the only vibration observed for the keto isomer, shows significant shortening of the O–N distance and suggesting that the ESIPT of P.Y.101 IS consistent with the skeletal deformation model.

### 3.3 Time-Resolved Infrared Spectra

We have shown that P.Y.101 in dichloromethane undergoes ESIPT by two time constants at 30 and 140 fs. Moreover, we demonstrated that TRF at high enough time resolution in conjunction with the theoretical calculation can be exploited for the identification of the emitting species through the vibrational spectrum obtained from the wave packet motion in time. The vibrational spectrum thus obtained is weighted by the Huang-Rhys factors between the two relevant states, which greatly assists the molecular assignment. To corroborate the conclusions, we also performed infrared transient absorption (IRTA) measurements.

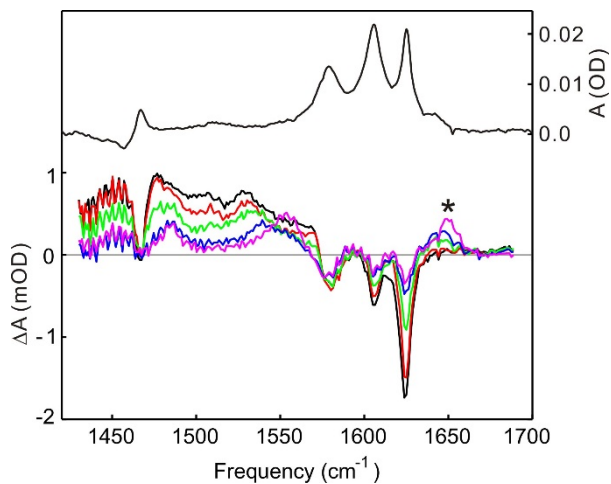


**Fig. 7** IRTA spectra of P.Y.101 in dichloromethane at 0.56 ps (black), 17.8 ps (red), 56 ps (green), 178 ps (blue), and 1 ns (magenta). Top figure shows the stationary infrared spectrum.

Fig. 7 shows the IRTA spectra of P.Y.101 in dichloromethane following excitation at 400 nm. The time resolution of the IRTA experiment was not high enough to resolve the ESIPT process directly. The spectra were measured for the frequency region corresponding to C=O and C=C stretching and N–H bending. In this region, frequencies of a vibrational mode for the ground enol, excited enol, and excited keto isomers are significantly different, unlike the skeletal vibrations in the low frequency region. The stationary infrared spectrum of P.Y.101 in this frequency region shows four major peaks at 1467, 1579, 1606, and 1625  $\text{cm}^{-1}$  (Table 3). Following the photoexcitation, these peaks show instrument limited bleach that persists for a 1 ns time window of the IRTA measurement. At the same time, broad and nearly featureless induced absorption bands in the 1420–1570  $\text{cm}^{-1}$  region were also observed. The 1606 and 1625  $\text{cm}^{-1}$  peaks of the ground enol isomer approximately correspond to the C=N stretching modes. The C=N bonds in the excited state weaken considerably to a bond order of  $\sim 1.5$ ,<sup>17</sup> and the vibrational frequencies downshift to  $\sim 1480 \text{ cm}^{-1}$ . Therefore, the induced absorption bands in the 1420–1570  $\text{cm}^{-1}$  region can be assigned to the infrared absorption bands of the excited enol and keto isomers.

Both bleach and the induced absorption bands decrease in tens of picoseconds indicating ground state recovery. However, the ground state recovery is not complete even at 1 ns, and  $\sim 25\%$  of the bleach remains along with several induced absorption bands. An IRTA and nanosecond laser flash photolysis study of P.Y.101 in the solid state has been reported previously by Staudt et al.<sup>16</sup> In that work, the bleach at 1625  $\text{cm}^{-1}$  lasts for 50  $\mu\text{s}$ , indicating that it comes from the dynamics in the ground state though the structure of the species was not identified. In addition, the 1650  $\text{cm}^{-1}$  band (marked \* in Fig. 7) did not appear in the solid state IRTA spectra, which implies that it may be related with a conformer such as the cis-keto or cis-enol isomer.

To obtain the dynamical information, we first fitted several regions of the IRTA data to a sum of exponentials. All regions of the IRTA data except the 1650  $\text{cm}^{-1}$  band can be described

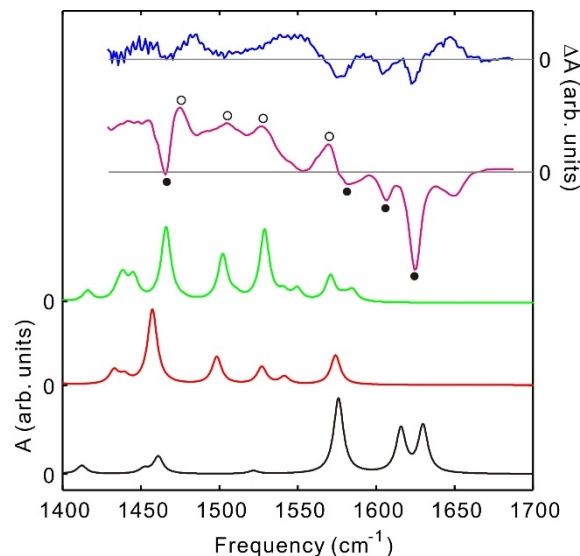


**Fig. 8** Top to bottom, DAS of  $\tau = \infty$  (blue), DAS of  $\tau = 62$  ps (magenta), calculated infrared absorption spectrum of excited keto (green), excited enol (red), and ground enol (black) isomers. Bleach bands (●) and induced absorption bands (○) are listed on the DAS of  $\tau = 62$  ps.

**Table 3.** Infrared absorption bands in 1400–1700  $\text{cm}^{-1}$  region.

Mode <sup>1)</sup>	IR	DAS <sup>2)</sup> (63 ps)	Calc. Gr. enol	Calc. Ex. enol	Calc. Ex. keto
$\nu_{93}$	1467	-1467	1461		
$\nu_{96}$ ( $\nu_{95}$ )		+1474		1457	1466
$\nu_{97}$ ( $\nu_{97}$ )		+1506		1498	1502
$\nu_{99}$ ( $\nu_{99}$ )		+1528		1527	1529
$\nu_{103}$ ( $\nu_{102}$ )		+1570		1574	1571
$\nu_{98}$	1579	-1580	1576		
$\nu_{102}$	1606	-1606	1616		
$\nu_{104}$	1625	-1624	1630		

<sup>1)</sup> Modes in parenthesis correspond to the excited keto isomer.

<sup>2)</sup> + and - signs represent induced absorption and bleach, respectively.

very well by two time constants: one at  $62 \pm 6$  ps, which can be regarded the same as the 67 ps time constant in TRF, and one much longer than 1 ns. The 1650  $\text{cm}^{-1}$  band shows a 240 ps rise that may be related to the conformational dynamics, but further interpretation was beyond the scope of the current work. We have also performed a global analysis to obtain the decay associated spectra (DAS).<sup>48</sup> Although we tried several different multi-exponential models, a bi-exponential model with time constants of 62 ps and infinity ( $\gg 1$  ns) provided satisfactory results and are consistent with the first analysis by exponential fits. A tri-exponential model produced time constants of 58 ps, 180 ps, and infinity with marginal decrease of the reduced  $\chi^2$  value. The DAS of  $\tau = 58$  ps was identical to the DAS of  $\tau = 62$  ps in the bi-exponential model, and the DAS of  $\tau = 180$  ps and infinity added up to give the DAS of  $\tau = \infty$  in the bi-exponential model. Since a time constant of 180 ps was not observed in any spectral region of the IRTA, we determined that the bi-exponential model is more appropriate.

Fig. 8 shows the DAS of  $\tau = 62$  ps and infinity and calculated infrared absorption spectra of the ground state enol, excited state

enol, and excited state keto isomers. Frequencies of all major bands are also listed in Table 3. The DAS of  $\tau = 62$  ps is quite similar to the IRTA spectrum obtained at 0.56 ps (Fig. 7). The DAS consists of four bleach bands and four induced absorption bands marked by the filled and open circles, respectively. The frequencies of the four bleach bands are, of course, the same as those of the stationary absorption bands, and they match well with the calculated infrared absorption spectrum of the enol isomer in the ground state. Although the induced absorption bands in the 1420–1570  $\text{cm}^{-1}$  region of the IRTA spectra are broad and nearly featureless, several induced absorption peaks can be identified in the DAS of  $\tau = 62$  ps. The induced absorption bands at 1474, 1506, 1528, and 1570  $\text{cm}^{-1}$  match well with the calculated infrared absorption spectrum of the excited keto isomer. However, the calculated infrared absorption spectra of the excited enol and keto isomers are too close to each other for us to confirm the absence of the excited enol isomer from the IRTA results alone. The fact that the bleach and the induced absorption peaks are time-independent (other than the 62 ps population relaxation) strongly suggests that all the dynamics including ESIPT is complete at 0.56 ps. This is consistent with the TRF results, where the ESIPT occurs in two time constants 30 and 140 fs.

#### 4. Conclusions

In this study, we presented time-resolved fluorescence (TRF) analyses of P.Y.101 in a dichloromethane solution. The TRF spectra over the entire emission wavelength and their area normalized representation showed that P.Y.101 undergoes ultrafast conversion from the initial photoexcited state to a different chemical species (or state) by two time constants of  $30 \pm 10$  and  $140 \pm 20$  fs, and possibly a third time constant of  $2.3 \pm 1$  ps. Such dispersive kinetics, that is, dynamics that cannot be characterized by a single rate constant, are frequently observed for chemical reactions in the liquid state.<sup>49</sup> In conjunction with the quantum chemical calculations, we concluded that this conversion is due to the excited state intramolecular proton transfer (ESIPT) process from trans-diol to trans-keto isomer. To positively identify the chemical species involved in this process, TRF were obtained with the highest time resolution at the fluorescence wavelengths corresponding to the two emitting states. Emission wavelength dependent vibrational spectra were obtained from the modulation of the TRF signals, which result from the wave packet motions on the excited state potential energy surfaces. All the wavelength dependent vibrational spectra can be represented by a sum of two spectra. With the help of quantum mechanical calculations, the two spectra were assigned to the vibrational spectra of the excited enol and keto isomers. Therefore, we were able to identify the two chemical species responsible for the emissions, and confirmed the ESIPT of P.Y.101. Time-resolved mid-infrared spectroscopy was also employed to corroborate the conclusion. At present, the time-resolution of the TRF experiment was limited to 50 fs, which limited the upper frequency of the vibrational spectrum to  $\sim 500$

$\text{cm}^{-1}$ . Further improvement on time resolution will be required to acquire the vibrational spectrum over a wider frequency range.

#### Acknowledgements

We thank Professor Reimer for providing the Dushin program. This work was supported by the National Research Foundation of Korea (NRF) grant funded by the Korea government (MEST) (2007-0056330) and the Global Research Laboratory Program (2009-00439). ML acknowledges the support from the National Research Foundation of Korea Grant funded by the Korean Government (NRF-2013S1A2A2035406).

#### Notes and references

<sup>a</sup> Department of Chemistry, Pohang University of Science and Technology (POSTECH), Pohang, 790-784, South Korea

<sup>b</sup> Department of Chemistry and Chemistry Institute for Functional Materials, Busan National University, Busan, 609-735, South Korea

<sup>†</sup> Electronic Supplementary Information (ESI) available: Picosecond TRF by TCSPC, Fourier transform of the residuals of the TRF signals, IRTA data at additional times, and numerical simulations of the TRF signal by convolution. See DOI: 10.1039/b000000x/

1. T. Joo, Y. W. Jia, J. Y. Yu, M. J. Lang and G. R. Fleming, *J. Chem. Phys.*, 1996, **104**, 6089.
2. S. Mukamel, *Principles of Nonlinear Optical Spectroscopy*, Oxford University Press, New York, 1999.
3. D. A. Farrow, A. Yu and D. M. Jonas, *J. Chem. Phys.*, 2003, **118**, 9348.
4. W. P. de Boeij, M. S. Pshenichnikov and D. A. Wiersma, *Chem. Phys. Lett.*, 1996, **253**, 53.
5. I. Eom and T. Joo, *J. Chem. Phys.*, 2009, **131**, 244507.
6. E. Riedle, M. Bradler, M. Wenninger, C. F. Sailer and I. Pugliesi, *Faraday Discuss.*, 2013, **163**, 139.
7. A. Weller, *Prog. React. Kinet.*, 1961, **1**, 188.
8. J. Goodman and L. E. Brus, *J. Am. Chem. Soc.*, 1978, **100**, 7472.
9. T. Elsaesser and W. Kaiser, *Chem. Phys. Lett.*, 1986, **128**, 231.
10. A. Douhal, F. Lahmani and A. H. Zewail, *Chem. Phys.*, 1996, **207**, 477.
11. D. McMorro and M. Kasha, *J. Phys. Chem.*, 1984, **88**, 2235.
12. A. Sytnik, D. Gormin and M. Kasha, *Proc. Natl. Acad. Sci. U. S. A.*, 1994, **91**, 11968.
13. A. Dreuw, A. Plötner, L. Lorenz, J. Wachtveitl, J. E. Djanhan, B. Brüning, T. Metz, M. Bolte and M. U. Schmidt, *Angew. Chem., Int. Ed.*, 2005, **44**, 7783.
14. J. Plötner and A. Dreuw, *Phys. Chem. Chem. Phys.*, 2006, **8**, 1197.
15. L. Lorenz, J. Plötner, V. V. Matyilitsky, A. Dreuw and J. Wachtveitl, *J. Phys. Chem. A*, 2007, **111**, 10891.
16. H. Staudt, T. Köhler, L. Lorenz, K. Neumann, M.-K. Verhoeven and J. Wachtveitl, *Chem. Phys.*, 2008, **347**, 462.
17. J. Plötner and A. Dreuw, *Chem. Phys.*, 2008, **347**, 472.
18. J. M. Jean and G. R. Fleming, *J. Chem. Phys.*, 1995, **103**, 2092.
19. C. Chudoba, E. Riedle, M. Pfeiffer and T. Elsaesser, *Chem. Phys. Lett.*, 1996, **263**, 622.
20. S. Lochbrunner, A. J. Wurzer and E. Riedle, *J. Chem. Phys.*, 2000, **112**, 10699.
21. S. Takeuchi and T. Tahara, *J. Phys. Chem. A*, 2005, **109**, 10199.

22. C. H. Kim and T. Joo, *Phys. Chem. Chem. Phys.*, 2009, **11**, 10266.
23. J. Ryu, H. W. Kim, M. S. Kim and T. Joo, *Bull. Korean Chem. Soc.*, 2013, **34**, 465.
24. C.-C. Hsieh, P.-T. Chou, C.-W. Shih, W.-T. Chuang, M.-W. Chung, J. Lee and T. Joo, *J. Am. Chem. Soc.*, 2011, **133**, 2932.
25. H. Rhee and T. Joo, *Opt. Lett.*, 2005, **30**, 96.
26. P. Manoj, C.-K. Min, C. T. Aravindakumar and T. Joo, *Chem. Phys.*, 2008, **352**, 333.
27. S. Kim, G. Jin and M. Lim, *J. Phys. Chem. B*, 2004, **108**, 20366.
28. M. J. Frisch, G. W. Trucks, H. B. Schlegel, G. E. Scuseria, M. A. Robb, J. R. Cheeseman, G. Scalmani, V. Barone, B. Mennucci, G. A. Petersson, H. Nakatsuji, M. Caricato, X. Li, H. P. Hratchian, A. F. Izmaylov, J. Bloino, G. Zheng, J. L. Sonnenberg, M. Hada, M. Ehara, K. Toyota, R. Fukuda, J. Hasegawa, M. Ishida, T. Nakajima, Y. Honda, O. Kitao, H. Nakai, T. Vreven, J. A. Montgomery, J. E. Peralta, F. Ogliaro, M. Bearpark, J. J. Heyd, E. Brothers, K. N. Kudin, V. N. Staroverov, R. Kobayashi, J. Normand, K. Raghavachari, A. Rendell, J. C. Burant, S. S. Iyengar, J. Tomasi, M. Cossi, N. Rega, J. M. Millam, M. Klene, J. E. Knox, J. B. Cross, V. Bakken, C. Adamo, J. Jaramillo, R. Gomperts, R. E. Stratmann, O. Yazyev, A. J. Austin, R. Cammi, C. Pomelli, J. W. Ochterski, R. L. Martin, K. Morokuma, V. G. Zakrzewski, G. A. Voth, P. Salvador, J. J. Dannenberg, S. Dapprich, A. D. Daniels, Farkas, J. B. Foresman, J. V. Ortiz, J. Cioslowski and D. J. Fox, *Gaussian 09, Revision B.01*, (2009) Gaussian, Inc, Wallingford CT.
29. J. Plötner, D. J. Tozer and A. Dreuw, *J. Chem. Theory Comput.*, 2010, **6**, 2315.
30. J. P. Merrick, D. Moran and L. Radom, *J. Phys. Chem. A*, 2007, **111**, 11683.
31. J. R. Reimers, *J. Chem. Phys.*, 2001, **115**, 9103.
32. C. Schrieffer, M. Barbatti, K. Stock, A. J. A. Aquino, D. Tunega, S. Lochbrunner, E. Riedle, R. de Vivie-Riedle and H. Lischka, *Chem. Phys.*, 2008, **347**, 446.
33. S. Lochbrunner, A. J. Wurzer and E. Riedle, *J. Phys. Chem. A*, 2003, **107**, 10580.
34. A. S. R. Koti, M. M. G. Krishna and N. Periasamy, *J. Phys. Chem. A*, 2001, **105**, 1767.
35. A. S. R. Koti and N. Periasamy, *J. Chem. Phys.*, 2001, **115**, 7094.
36. Although TCSPC gave 73 ps, we used 67 ps obtained from the femtosecond TRF experiment, since it was close to the instrument response of the TCSPC apparatus.
37. M. L. Horng, J. A. Gardecki, A. Papazyan and M. Maroncelli, *J. Phys. Chem.*, 1995, **99**, 17311.
38. M. J. Rosker, F. W. Wise and C. L. Tang, *Phys. Rev. Lett.*, 1986, **57**, 321.
39. I. A. Walmsley, M. Mitsunaga and C. L. Tang, *Phys. Rev. A*, 1988, **38**, 4681.
40. H. Barkhuijsen, R. De Beer, W. M. M. J. Bovee and D. Van Ormondt, *J. Magn. Reson.*, 1985, **61**, 465.
41. F. W. Wise, M. J. Rosker, G. L. Millhauser and C. L. Tang, *IEEE J. Quantum Electron.*, 1987, **23**, 1116.
42. I. Eom, S. Park, H.-S. Han, K.-J. Yee, S.-H. Baik, D.-Y. Jeong, T. Joo and Y.-S. Lim, *Nano Lett.*, 2012, **12**, 769.
43. M. Higashi and S. Saito, *J. Phys. Chem. Lett.*, 2011, **2**, 2366.
44. R. de Vivie-Riedle, V. De Waele, L. Kurtz and E. Riedle, *J. Phys. Chem. A*, 2003, **107**, 10591.
45. J. Lee, C. H. Kim and T. Joo, *J. Phys. Chem. A*, 2013, **117**, 1400.
46. P. Kukura, D. W. McCamant and R. A. Mathies, *Annu. Rev. Phys. Chem.*, 2007, **58**, 461.
47. F. Han, W. Liu and C. Fang, *Chem. Phys.*, 2013, **422**, 204.
48. C. Ruckebusch, M. Sliwa, P. Pernot, A. de Juan and R. Tauler, *J. Photochem. Photobiol. C: Photochem. Rev.*, 2012, **13**, 1.
49. C. H. Kim, D. W. Chang, S. Kim, S. Y. Park and T. Joo, *Chem. Phys. Lett.*, 2008, **450**, 302.